Study on the Color-Compensation Effect of Hybrid Orange-Red Quantum Dots in WLED Application

Xiaoyue Hu
Hebei University of Technology
Yangyang Xie
Hebei University of Technology
Chong Geng
Hebei University of Technology
Shu Xu (shu.xu@hebut.edu.cn)
Hebei University of Technology https://orcid.org/0000-0002-4185-1392
Wengang Bi
Hebei University of Technology

Nano Express

Keywords: quantum dots, spectral control, lifetime, quantum efficiency, energy transfer

Posted Date: February 14th, 2020

DOI: https://doi.org/10.21203/rs.2.23549/v1

Abstract

Quantum dots (QDs) as emerging light-converting materials show the advantage of enhancing color quality of white light-emitting diode (WLED). However, WLEDs employing narrow-emitting monochromic QDs usually present unsatisfactory color rendering in the orange region. Herein, orange-red emitting polychromic hybrid QDs (hybrid-QDs) are developed through mixing CdSe/ZnS based orange QDs (O-QDs) and red QDs (R-QDs) to compensate the orange-red light for WLEDs. We investigated the effect of self-absorption and fluorescence resonance energy transfer (FRET) process in hybrid-QDs on the spectral controllability and fluorescent quenching in WLEDs. The concentration and donor/acceptor ratios were also taken into account to analyze the FRET efficiency and help identify suitable hybrid-QDs for color compensation in the orange-red light region. As the result, the optimized hybrid-QDs effectively improve the color rendering index of the WLED compared with monochromatic QDs at the same color coordinates.

1. Introduction

Light-emitting diodes (LEDs) have attracted significant research interests in solid-state lighting applications due to their high efficiency, long lifetime, low-power consumption, fast response time and high reliability [1, 2, 3, 4, 5, 6]. WLEDs are usually fabricated by packaging yellow, green and red-emitting phosphors with blue-LED chips [7, 8, 9]. The full-spectrum WLEDs employ hybrid phosphors with a high proportion of red phosphor [10]. However, classical red phosphors have a broad emission that causes lumen loss in the red-light emitting region because the human eye is insensitive to the wavelength longer than 650 nm [11].

Recently, quantum dots (QDs) have been employed to fabricate high-quality WLEDs. Compared to classical phosphors, QDs have unique optical properties, such as size-dependent wavelength tunability, high photoluminescence quantum yield and strong absorption [12, 13, 14, 15, 16, 17]. Because of the narrow emitting characteristics at red-light region, the red-emitting QDs are particularly useful for inhibiting the above-mentioned lumen loss and improving color rendering index (CRI) of WLEDs [18, 19]. Therefore, using QDs to compensate for the orange-red region has become an effective measure for enhancing the color quality of WLEDs [20]. Generally, QD-based WLEDs (QWLEDs) can be divided into two categories by mixing monochromic or polychromatic QDs in the LEDs [20, 21, 22, 23]. For example, Xie et al. used red-emitting CdSe/CdS/ZnS QDs to replace classical red phosphor with LuAG:Ce green phosphor to fabricate high performance WLED [24]. Li et al. fabricated QWLEDs by integrating a mixture of red, yellow and green light-emissive CdZnS/ZnSe QDs on the blue-emitting GaN LED chip, which exhibited a CRI of 85.2 and correlated color temperature (CCT) of 4072 K [25].

To date, the full spectrum QWLEDs for lighting application are commonly developed by incorporating broad emitting green-yellow phosphors and narrow emitting monochromatic red QDs [24]. These QWLEDs present superb spectral continuity in the green-yellow region but a clear valley in the orange-red region. Theoretically, a hybrid QDs made of several monochromic QDs in the orange-red region are capable to fill the valley and further improve the spectral continuity of QWLEDs. However, it is difficult to

regulate the spectra of the hybrid QDs because of the self-absorption and fluorescence resonance energy transfer (FRET) process among polychromatic QDs [26]. Therefore, although the color property of the QWLEDs have been investigated by manipulating the peak position and broadness of the monochromatic red QDs, the hybrid orange-red QDs have not been studied in WLEDs on account of the self-absorption and FRET process.

Herein, hybrid orange-red QDs were studied to enhance the spectral continuity and color quality of the orange-red light-emitting region for QWLEDs. We prepared CdSe/ZnS based orange QDs (O-QDs) and red QDs (R-QDs) with different full width at half maximum (FWHM) as the component of the hybrid orange-red QDs (hybrid-QDs). The FRET in the hybrid-QDs was studied by considering the effects of concentration and proportion of hybrid-QDs. The results were used to optimize the quantum efficiency (QE) and spectral controllability of the hybrid-QDs. Moreover, the hybrid orange-red QDs were used with LuAG:Ce green phosphor in blue LEDs to form QWLEDs. The as-prepared QWLEDs exhibit enhanced color quality with a more balanced full spectrum in the orange-red region.

2. Methods

Materials and Chemicals

1-Octadecene (ODE, 90%), sulfur (S, 98.5%), trioctylphosphine (TOP, 85%), and stearic acid (98%) were purchased from TCI (Shanghai). Cadmium stearate ($Cd(St)_2$) was purchased from Shanghai Debo Chemical Technology Co., Ltd. Selenium powder (Se, 325 mesh, 99.5%) was purchased from Alfa Aesar (China). Zinc acetate ($Zn(Ac)_2$, 99.5%) was purchased from Shanghai Titan Scientific Co., Ltd. Ethanol (AR) and dimethylbenzene were purchased from Tianjin Damao Chemical Reagent Co., Ltd. Silicone resin (Dow Corning-6662) was from Shineon Co., Ltd. Other materials are shown in the manuscript. All chemicals were used directly without any further purification unless otherwise stated.

Synthesis of O-QDs.

The synthetic procedure was based on the report in the literature [27]. $Cd(St)_2$ (2 mmol) and stearic acid (0.2 mmol) were loaded into a 50 mL three-neck flask with 10 mL of ODE. After stirring with nitrogen bubbling, the solution was heated to 270 °C. Then 0.5 mL of TOP-Se (2 mmol of Se powder dissolved in 1 mL of TOP) was rapidly injected into the flask and maintained at 270 °C for 2 min. Afterward, 0.5 mL of TOP-S (4 mmol of S powder dissolved in 2 mL of TOP, stirred well) was rapidly injected into the flask and maintained at 270 °C for 40 min, and then the flask was cooled to 30 °C. $Cd(St)_2$ (0.75 mmol), $Zn(Ac)_2$ (2.25 mmol), and 5 mL of ODE were added into the above solution. After stirring with nitrogen bubbling, the flask was heated to 160 °C. 1.5 mL of TOP-S was slowly injected into the flask and maintained at 160 °C for 4 h, and then the flask was cooled to room temperature. After a centrifuged purification procedure with ethanol, the as-prepared CdSe/ZnS QDs were dispersed in 10 mL of dimethylbenzene for further use.

Synthesis of R-QDs.

The synthetic procedure was similar to that of O-QDs expect for the following two points. The heating temperature adjusted from 270 to 300 °C. And the second added $Cd(St)_2$ is 1 mmol together with $Zn(Ac)_2$ (3 mmol).

Preparation of O-QDs and R-QDs silicone gel thin films

Different weights of R-QDs were homogeneously mixed into the same volume silicone gels to build the different concentration R-QDs gels (0.05, 0.1, 0.2, 0.4, 0.8, 2, 4, and 10 mg/mL). Then, different concentrations of R-QDs gels with the same volume were added into the same type of molds and removed the bubbles. Finally, the R-QDs-silicone composite thin films were built by curing at 150 °C for 60 min. The O-QDs-silicone thin films are fabricated by the same process with different concentrations (0.05, 0.1, 0.2, 0.4, 0.8, 2, 4, 10, and 14 mg/mL).

Preparation of hybrid orange-red QDs silicone gel thin films with different weight ratios of O-QDs:R-QDs.

The hybrid orange-red QDs silicone gel with different weight ratios of O-QDs:R-QDs (10:1, 5:1, 5:2, and 5:4) were prepared by homogeneously mixing the as-prepared O-QDs gel (10 mg/mL) and R-QDs gel (2 mg/mL) with different volume ratios (2:1, 1:1, 1:2 and 1:4). Then, the different concentrations of hybrid-QDs gels were added into the same type of mold and removed the bubbles. Finally, the hybrid-QDs silicone gel thin films were built by curing at 150 °C for 1 h.

Preparation of hybrid-QDs silicone gel thin films

With the same weight ratio of O-QDs:R-QDs (10:1), the hybrid-QDs were mixed into the different volumes of silicone gels to form hybrid-QDs gels with different concentrations (0.35, 0.5, 0.75, 1, 1.5 and 3 mg/mL). Then, the as-prepared hybrid-QDs gels were added into the same type of molds and removed the bubbles. Finally, the hybrid-QDs silicone gel thin films with different hybrid-QDs concentrations were built by curing at 150 °C for 1 h.

Fabrication of WLEDs

The LED chips (typical 2835 lead frame package) with the emission peak at 450 nm were used for the fabrication of WLEDs.

Green-emitting LuAG:Ce phosphor, O-QDs (10 mg/mL), R-QDs (2 mg/mL) or hybrid O-R QDs (weight ratio 10:1) were mixed homogeneously with silicone gel (Dow Corning 6662, A:B = 1:4), and the mixture was degassed under vacuum. With a common packaging method based on silicone gel, the four different WLEDs were developed with LuAG:Ce phosphor, phosphor & O-QDs, phosphor & R-QDs, and phosphor & hybrid-QDs, respectively. Finally, the above WLEDs were cured by curing at 150 °C for 1 h.

Measurement and Characterization

Photoluminescence (PL) was recorded on an Ideaoptics FX2000-EX PL spectrometer. Transmission electron spectroscopy (TEM) was performed on a FEI Tecnai G2 Spirit TWIN transmission electron microscope operating at 100 kV. The quantum efficiency (QE) measurements were carried out on an OceanOptics QEpro QY test system under 365 nm blue laser irradiation. The luminous efficiency and optical power were recorded on an EVERFINE ATA-1000 LED automatic temperature control photoelectric analysis and measurement system. UV-Vis absorption was measured by using a Persee T6 UV-Vis spectrometer. The excitation spectra and time-resolved PL spectroscopy (TRPL) have been measured by an Edinburgh FLS920 fluorescence spectrometer.

3. Results And Discussion

The optical properties of the two monochromic QDs were firstly studied. Figure 1a and b show the photoluminescence (PL) and absorption spectra of the R-QDs and O-QDs. The FWHM of the R-QDs and O-QDs is about 20.6 and 43 nm, respectively. The positions of dotted lines indicate the PL and absorption peaks. As shown in TEM images, the R-QDs and O-QDs exhibit a cubic morphology with an average size of 13 nm and 12 nm (Fig. 1c and d), respectively. The inset HRTEM images show an interplanar distance of 0.35 nm, which can be assigned to the (111) plane of the cubic phase ZnS.

The optical properties of QDs-silicone thin films made of the monochromic R-QDs and O-QDs with different concentrations are further tested under excitation by a 365 nm laser at 15.88 mW/cm^2. Figure 2a and b show the concentration dependent PL spectra of the QDs and their FWHM is almost constant. Figure 2c and d exhibit the PL intensity and absolute QE of monochromic QDs-silicone thin films with different concentrations of QDs. With the rise of concentration, the PL intensity of R-QDs silicone thin films increases until the QD concentration reaches 2 mg/mL and then decreases because of concentration quenching. Similar to the variation in PL intensity, the QE of the QDs reaches the highest value of about 85% at the same concentration. The PL intensity and QE of the O-QDs silicone thin films present a similar concentration dependent trend compared to those of the R-QDs based thin films. Differently, the PL intensity and QE of the O-QDs rise quickly till a QD concentration of 4 mg/mL and the maximum values are obtained at the concentration of 10 mg/mL. We infer that it is attributed to the larger Stoke's shift of the O-QDs than the R-QDs. The maximum QE of the O-QDs silicone thin film is about 76%, which is at the same QD concentration for the highest PL intensity.

Moreover, the 2 mg/mL R-QDs and 10 mg/mL O-QDs based silicone gel films also exhibit the highest PL intensity under different exciting power, as shown in Fig. S1 a and b, respectively. At the above two concentrations, the optical properties of the monochromic QDs are effectively preserved, which weakens the PL quenching caused by the host matrix effect [28, 29]. The study helps to find the suitable concentration of the monochromic QDs in silicone film.

To further investigate the concentration influence of QDs in the monochromic QDs based silicone thin films, the time-resolved PL (TRPL) spectra of the thin films with different concentrations are measured

and the decay curves are depicted in Fig. 3. It is known that PL decay curves can be expressed with a multi-exponential function, as illustrated by Eq. 1 [30],

$$I(t) = \sum_{i=1}^{n} A_i e^{-t/\tau_i} \quad (1)$$

where I(t) is the PL intensity at time t. Ai and τi represent the relative amplitude and the excited state lifetime of each exponential component of PL decay, n is the number of decay times. These decay curves, as shown in Fig. 3a and b, can be well fitted by a double exponential function according to Eq. 1.

The fitting parameters Ai and τi are listed in Table S1 and S2. The amplitude-weighted lifetimes of the R-QDs and O-QDs are selected as their lifetimes (τ_{ave}) for further investigation. The lifetime can be calculated from the following Eq. 2 [31] and is listed in Table S1 and S2.

$$\tau_{ave} = \frac{A_1\tau_1 + A_2\tau_2}{A_1 + A_2} \quad (2)$$

Figure 3c and d show the lifetimes of the two monochromic QDs under different concentrations. Both lifetimes increase with the rise of concentrations and the rising rate becomes slower after 1 mg/mL for the R-QDs and 2 mg/mL for the O-QDs, respectively. It indicates that the rise of concentration reduces the distance amongst QDs thus enhances the energy transfer and self-absorption in the monochromic QDs [32, 33]. Meanwhile, the increment of the lifetime in O-QDs is more obvious than that in R-QDs, suggesting more energy transfer in O-QDs. However, it appears that the energy transfer does not induce fluorescent quenching of the QDs at low concentration. On the contrary, it may have positive effect on the PL intensity and QEs, as previous shown in Fig. 2.

The optical properties of hybrid orange-red QDs with different weight ratios of R-QDs:O-QDs were further studied. The PL spectra of the hybrid-QDs thin films are shown in Fig. 4a. Based on the spectra, the hybrid-QDs PL peak intensity ratio of 631:605 (nm) is extracted in Fig. 4b. The peak intensity ratio presents a rising increment with the R-QDs percentage, which suggests the energy transfer from O-QDs to R-QDs. Figure 4c exhibits the overlap between the R-QDs absorption spectrum and the O-QDs emission spectrum. It suggests a high chance of FRET process, in which the O-QDs acts as the donor and R-QDs as the acceptor (shown in Fig. 4d).

Further study focuses on the FRET process in hybrid-QDs. Figure 5a presents the effect of R-QDs (acceptor) on the emission kinetics of the O-QDs (donor). The TRPL intensity decreases with the rise of acceptor in the film sample (analyzed at peak donor emission wavelength 605 nm). Figure 5b presents the effect of O-QDs (donor) on the emission kinetics of the R-QDs (acceptor). On the contrary, the TRPL intensity increases with the rise of the donor in the film sample (analyzed at peak acceptor emission wavelength 631 nm). The decay curves in Fig. 5a and b can be fitted with the 2 exponentials, and the detailed amplitudes, lifetime components, and amplitude-weighted lifetimes of the QDs were listed in Table S3. The lifetime of the O-QDs sample was found to be 30.25 ns. When the acceptor R-QDs are

introduced, the lifetime of the donor O-QDs decreases (Table S3) owing to the intervene of the energy-transferring channel. The lifetime of the donor becomes shorter with the rise of the acceptor concentration. On the contrary, the lifetime of the R-QDs sample was found to be 13.08 ns. When the donor O-QDs are introduced, the acceptor R-QDs present an increase in lifetime as a result of energy feeding (Table S3) [34]. The calculated results are shown in Fig. 5c, which clearly demonstrates the phenomena.

The FRET process is also investigated by energy transfer efficiency. The efficiency of FRET can be calculated according to lifetime as illustrated by Eq. 3.

$$E = 1 - \frac{\tau_{DA}}{\tau_D} \quad (3)$$

Where τ_{DA} is the donor fluorescence lifetime in the presence of the acceptor, τ_D is the donor fluorescence lifetime in the absence of acceptor [26]. It shows that τ_{DA} is inversely proportional to the energy transfer efficiency. Therefore, as the acceptor-donor ratio increases, the τ_{DA} becomes shorter and the energy transfer efficiency increases. Larger energy transfer efficiency reflects higher impact on fluorescence. We further analyze the FRET efficiency of hybrid-QDs in Fig. 5a. The calculated results are listed in Table 1 and the efficiency reaches 33.2% with the highest proportion of acceptor. Meanwhile, Fig. 5d exhibits the change of FRET efficiency under different ratios of donor-to-acceptor. The FRET efficiency increases with the rise of R-QDs (acceptor) in the hybrid-QDs and the increment rate of the efficiency is close to that of the R-QDs. It indicates that the increment of energy transfer is sensitive to the increment of the acceptor.

Table 1 FRET efficiency of hybrid-QDs silicone thin films with different ratios of acceptor-to-donor.

R-QDs:O-QDs (acceptor:donor)	τ_{DA}	E
	9	
Only O-QDs	30.25 (τ_D)	--
1:10	27.96	7.6%
1:5	27.29	9.8%
2:5	24.93	17.6%
4:5	20.2	33.2%

As the best continuity spectrum for LED lighting in orange-red light, the hybrid-QDs with the 1:10 weight ratio of R-QDs:O-QDs is selected for further study. Fig. 6a exhibits the PL spectra of the hybrid-QDs silicone thin films with different concentrations of hybrid-QDs at the same weight ratio of R-QDs:O-QDs (R:O=1:10). Besides the increase of the overall PL intensity, the proportion of the red-light (631 nm) also increases obviously with the rise of the QD concentration, as shown in Fig. 6b. This phenomenon can be attributed to the enhanced FRET with increasing QD concentration. Moreover, the rising rate of the red light becomes slower at higher QD concentration. This could be due to the saturation of the energy transfer (ET) amongst QDs. However, the absolute QEs of the QD-silicone composite thin films exhibits a less than 5% change with different concentrations of hybrid-QDs, as shown in Fig. 6c. It appears that 1.0-

1.5 mg/mL is the most favourable QD concentration for hybrid QDs in application, which ensures high QEs with a low spectrum variation.

The TRPL decay curves of the different hybrid-QDs concentration thin films are shown in Fig. S2. Table S4 lists the amplitudes, lifetime components, and amplitude-weighted lifetimes for the hybrid-QDs in Fig. S2. Their FRET efficiencies are calculated and shown in Table S5. Furthermore, the changes in lifetimes and FRET efficiency with concentration are clearly shown in Fig.6d. In detail, the FRET efficiency exhibits a decrement trend from 22% to 9% with the rise of concentration. Meanwhile, the lifetime recorded at the emission wavelength of the donor O-QDs increases with increasing concentration (orange dots in Fig. 6d). This is similar to the concentration dependent lifetime of the pure O-QDs samples shown in Fig.3. It suggests the existence of the combined effect of FRET and self-absorption (like the monochrome QDs). With the rise of concentration, the enhanced self-absorption leads to the increment of the τ_{DA} (the donor fluorescence lifetime in the presence of the acceptor, as shown in Fig. 6d, orange dots), suggesting the inhibition of the FRET between hybrid QDs (blue dots in Fig. 6d). At the acceptor R-QDs emission wavelength, the reduced FRET efficiency results in smaller increment of the lifetime in high concentration (red dots in Fig. 6d). As a result, the hybrid-QDs show relative weak concentration dependent lifetimes and could maintain a stable QE, which benefits the application of hybrid-QDs in LED applications.

To study the light compensation effect of the hybrid-QDs in lighting application, WLEDs are fabricated by mixing green-emitting LuAG:Ce phosphor and O-QDs, R-QDs or hybrid-QDs (R:O=1:10) and packaging the mixture on top of 450 nm emitting GaN chips. Under a driving current of 40 mA, the excitation-luminescence (EL) spectra of the as-prepared WLEDs are illustrated in Fig. 7. The correlated color temperature (CCT) and color coordinates of the WLEDs are shown in Fig. S3 and Table S6. The four WLEDs have almost the same spectra in blue-green light region but different in the orange-red light region. Besides, the LuAG:Ce (only) based WLED shows the lowest color rendering index (CRI) of 48.8 due to the loss of red-orange light region. On the contrary, the hybrid-QDs based WLED exhibits a broader and flat spectrum in the orange-red light region and the highest CRI of 92.1. Compared to the hybrid-QDs, the LuAG:Ce (only) and R-QDs based WLEDs present obvious light gap in the orange light region and show great differences in CCT and color coordinates. Although the O-QDs based WLED has the similar CCT and color coordinates with the hybrid-QDs based WLED, it lacks the red light and thus presents a much lower CRI than that of the hybrid-QDs. It indicates the promising ability of hybrid orange-red QDs in enhancing the color quality of WLED.

4. Conclusion

In summary, we prepared the hybrid orange-red QDs and studied their optical properties and the energy transfer dynamic in the hybrid-QDs for LED applications. Our study reveals that the concentration of the hybrid-QDs and the proportion of donor-QDs and receptor-QDs play an important role in the energy transfer efficiency and spectrum stability. Meanwhile, the self-absorption has a significant influence on the FRET between different monochromic QDs in the hybrid-QDs. The relative stable and high QE can be achieved by adjusting the donor-to-receptor ratio in the hybrid-QDs, which is meaningful to enhance the

color quality of WLED by compensation of the light gap in the orange-red region. As a result, the WLED fabricated based on the hybrid-QDs exhibits a highly improved color quality and more natural light spectrum compared to the spectra of the monochromic-QDs based WLEDs.

5. Abbreviations

QDs: Quantum dots; WLEDs: White light-emitting diodes; hybrid-QDs: orange-red emitting polychromic hybrid QDs; O-QDs: CdSe/ZnS based orange QDs; R-QDs: CdSe/ZnS based red QDs; FWHM: Full width at half maximum; FRET: Fluorescence resonance energy transfer; LEDs: Light-emitting diodes; CRI: Color rendering index; QWLEDs: QD-based WLEDs; CCT: Correlated color temperature; QE: Quantum efficiency; ODE:1-octadecence; S: sulfur; TOP: Trioctylphosphine; Cd(St)2: Cadmium stearate; Se: Selenium powder $Zn(Ac)_2$: Zinc acetate; AR: Ethanol ; PL: Photoluminescence; TEM: Transmission electron spectroscopy; TRPL: Time-resolved PL spectroscopy; EL: excitation-luminescence.

6. Declarations

Acknowledgements

This work was financially supported by the National Key R&D Program of China (2016YFB0400600, 2016YFB0400605), National Natural Science Foundation of China (Nos. 51672068, 51902082), Natural Science Foundation of Tianjin City (No. 17JCYBJC41500), and Graduate Innovation Foundation of Hebei Province (No. CXZZBS2018031).

Funding

National Key R&D Program of China (2016YFB0400600, 2016YFB0400605), National Natural Science Foundation of China (Nos. 51672068, 51902082), Natural Science Foundation of Tianjin City (No. 17JCYBJC41500) and Graduate Innovation Foundation of Hebei Province (No. CXZZBS2018031).

Availability of Data and Materials

The datasets generated during and/or analyzed during the current study are available from the corresponding authors on reasonable request.

Authors’ Contributions

XH, SX, and WB conceived and designed the experiments. YX provided the quantum dot material. XH performed the experiments. XH, SX and YX analyzed the data. CG contributed the analysis tools. XH wrote the manuscript and SX improved the manuscript. All authors read and approved the final manuscript.

Competing Interests

The authors declare that they have no competing interests.

References

1. Lee KH, Han CY, Kang HD et al (2015) Highly efficient, color-reproducible full-color electroluminescent devices based on red/green/blue quantum dot-mixed multilayer. ACS nano 9: 10941-10949
2. Lita A, Washington AL, van de Burgt L et al (2010) Stable Efficient Solid-State White-Light-Emitting Phosphor with a High Scotopic/Photopic Ratio Fabricated from Fused CdSe-Silica Nanocomposites. Adv Mater 22: 3987-3991
3. Jun S, Lee J, Jang E (2013) Highly luminescent and photostable quantum dot–silica monolith and its application to light-emitting diodes. Acs Nano 7: 1472-1477
4. Jang HS, Yang H, Kim SW et al (2008) White light-emitting diodes with excellent color rendering based on organically capped CdSe quantum dots and Sr_3SiO_5: Ce^{3+}, Li^+ phosphors. Adv Mater 20: 2696-2702
5. Yang X, Zhao D, Leck KS et al (2012) Full visible range covering InP/ZnS nanocrystals with high photometric performance and their application to white quantum dot light-emitting Diodes. Adv Mater 24: 4180-4185
6. Park SH, Hong A, Kim JH et al (2015) Highly bright yellow-green-emitting $CuInS_2$ colloidal quantum dots with core/shell/shell architecture for white light-emitting diodes. ACS Appl Mater Interfaces 7: 6764-6771
7. Xia Z, Zhang Y, Molokeev MS et al (2013) Structural and luminescence properties of yellow-emitting $NaScSi_2O_6$: Eu^{2+} phosphors: Eu^{2+} site preference analysis and generation of red emission by codoping Mn^{2+} for white-light-emitting diode applications. J Phys Chem C 117: 20847-20854
8. Wu H, Zhang X, Guo C et al (2005) Three-band white light from InGaN-based blue LED chip precoated with green/red phosphors. IEEE Photonic Tech L 17: 1160-1162
9. Kimura N, Sakuma K, Hirafune S et al (2007) Extrahigh color rendering white light-emitting diode lamps using oxynitride and nitride phosphors excited by blue light-emitting diode. Appl Phys Lett 90: 051109
10. Xie RJ, Hirosaki N, Kimura N et al (2007) 2-phosphor-converted white light-emitting diodes using oxynitride/nitride phosphors. Appl Phys Lett 90: 191101
11. Mueller-Mach R, Mueller G, Krames MR et al (2005) Highly efficient all-nitride phosphor-converted white light emitting diode. Phys solidi a 202: 1727-1732
12. Bae WK, Lim J, Lee D et al (2014) R/G/B/natural white light thin colloidal quantum dot-based light-emitting devices. Adv Mater 26: 6387-6393
13. Fitzmorris BC, Cooper JK, Edberg J et al (2012) Synthesis and structural, optical, and dynamic properties of core/shell/shell CdSe/ZnSe/ZnS quantum dots. J Phys Chem C 116: 25065-25073

14. Schlegel G, Bohnenberger J, Potapova I et al (2002) Fluorescence decay time of single semiconductor nanocrystals. Phys Rev Lett 88: 137401
15. Kigel A, Brumer M, Maikov GI et al (2009) Thermally activated photoluminescence in lead selenide colloidal quantum dots. Small 5: 1675-1681
16. Wang X, Qu L, Zhang J et al (2003) Surface-related emission in highly luminescent CdSe quantum dots. Nano Lett 3: 1103-1106
17. Zhang J, Zhang X, Zhang JY (2009) Size-dependent time-resolved photoluminescence of colloidal CdSe nanocrystals. J Phys Chem C 113: 9512-9515
18. Woo JY, Kim KN, Jeong S et al (2010) Thermal behavior of a quantum dot nanocomposite as a color converting material and its application to white LED. Nanotechnology 21: 495704
19. Bi W, Xu S, Geng C et al (2016) Quantum dots enabled LCD displays and solid-state lighting//Low-Dimensional Materials and Devices. Proc of SPIE 9924: 992403
20. Lin HY, Wang SW, Lin CC et al (2015) Excellent color quality of white-light-emitting diodes by embedding quantum dots in polymers material. IEEE J Sel Top Quant 22: 35-41
21. Song WS, Yang H (2012) Fabrication of white light-emitting diodes based on solvothermally synthesized copper indium sulfide quantum dots as color converters. Appl Phys Lett 100: 183104
22. Song WS, Yang H (2012) Efficient white-light-emitting diodes fabricated from highly fluorescent copper indium sulfide core/shell quantum dots. Chem Mater 24: 1961-1967
23. Huang B, Dai Q, Zhuo N et al (2014) Bicolor Mn-doped $CuInS_2$/ZnS core/shell nanocrystals for white light-emitting diode with high color rendering index. J Appl Phys 116: 094303
24. Xie Y, Geng C, Liu X et al (2017) Synthesis of highly stable quantum-dot silicone nanocomposites via in situ zinc-terminated polysiloxane passivation. Nanoscale 9: 16836-16842
25. Li F, You L, Li H et al (2017) Emission tunable CdZnS/ZnSe core/shell quantum dots for white light emitting diodes. J Lumin 192: 867-874
26. Altıntas Y, Talpur MY, Mutlugün E (2017) Efficient Forster resonance energy transfer donors of In (Zn) P/ZnS quantum dots. J Phys Chem C 121: 3034-3043
27. Xie Y, Yang D, Zhang L et al (2019) Highly Efficient and Thermally Stable QD-LEDs Based on Quantum Dots-SiO_2-BN Nanoplate Assemblies. ACS Appl Mater Interfaces 12: 1539-1548
28. Park HC, Gong S, Cho YH (2017) How Effective is Plasmonic Enhancement of Colloidal Quantum Dots for Color-Conversion Light-Emitting Devices? Small 13: 1701805
29. Su CY, Lin CH, Yao YF et al (2017) Dependencies of surface plasmon coupling effects on the p-GaN thickness of a thin-p-type light-emitting diode. Opt Express 25: 21526-21536
30. Xing W, Zhang X, Geng C et al (2019) Multi-quantum-well quantum dots with stable dual emission. Nanoscale 11: 8475-8484
31. Lakowicz JR (2013) Principles of fluorescence spectroscopy. Springer Science &Business Media
32. Santra PK, Kamat PV (2012) Mn-doped quantum dot sensitized solar cells: a strategy to boost efficiency over 5%. J Am Chem Soc 134: 2508-2511

33. Wang X, Yan X, Li W et al (2012) Doped quantum dots for white-light-emitting diodes without reabsorption of multiphase phosphors. Adv Mater 24: 2742-2747
34. Guzelturk B, Olutas M, Delikanli S et al (2015) Nonradiative energy transfer in colloidal CdSe nanoplatelet films. Nanoscale 7: 2545-2551

Figures

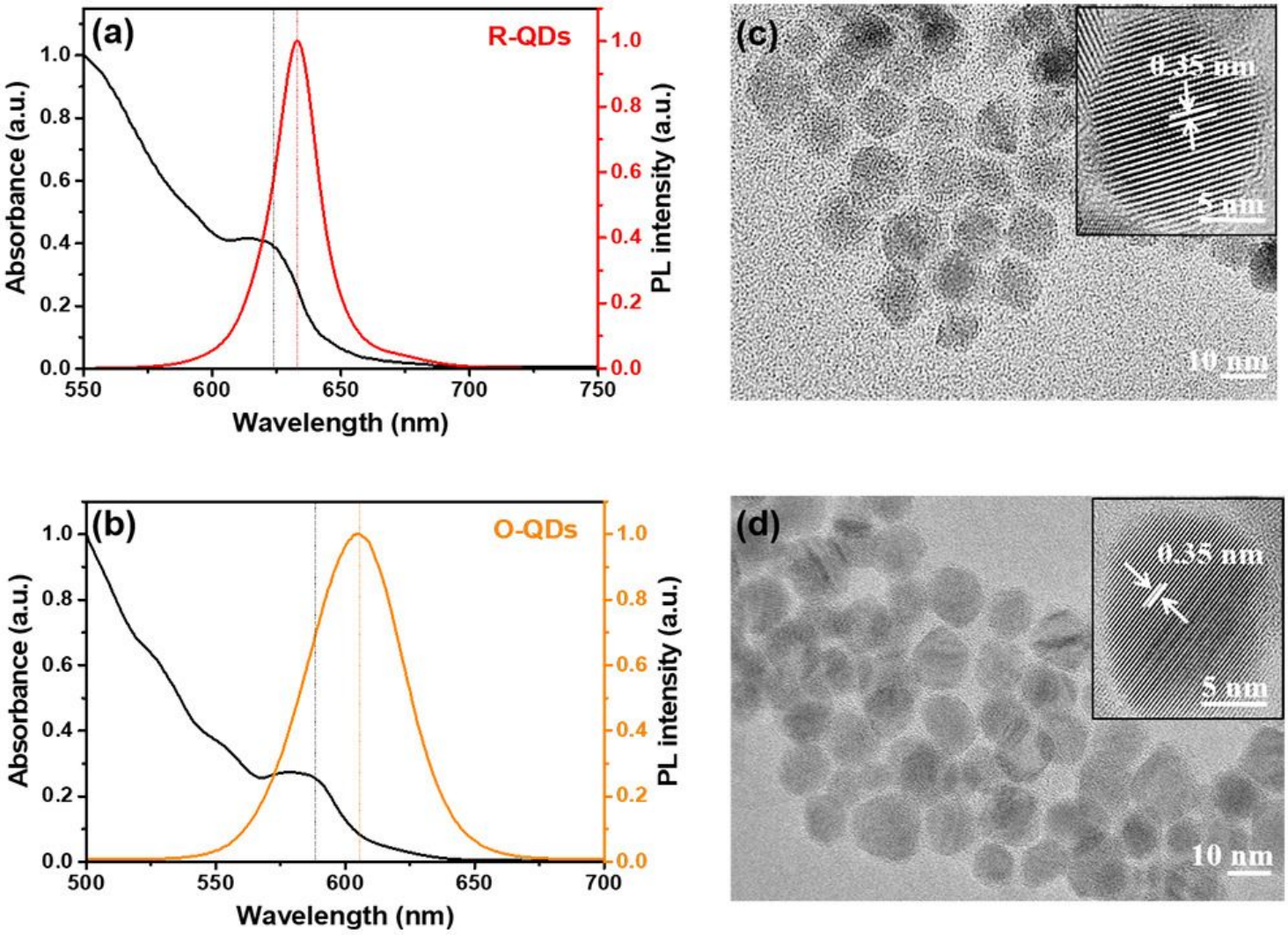

Figure 1

PL and UV spectra of R-QDs (a) and O-QDs (b). TEM images of R-QDs (c) and O-QDs (d).

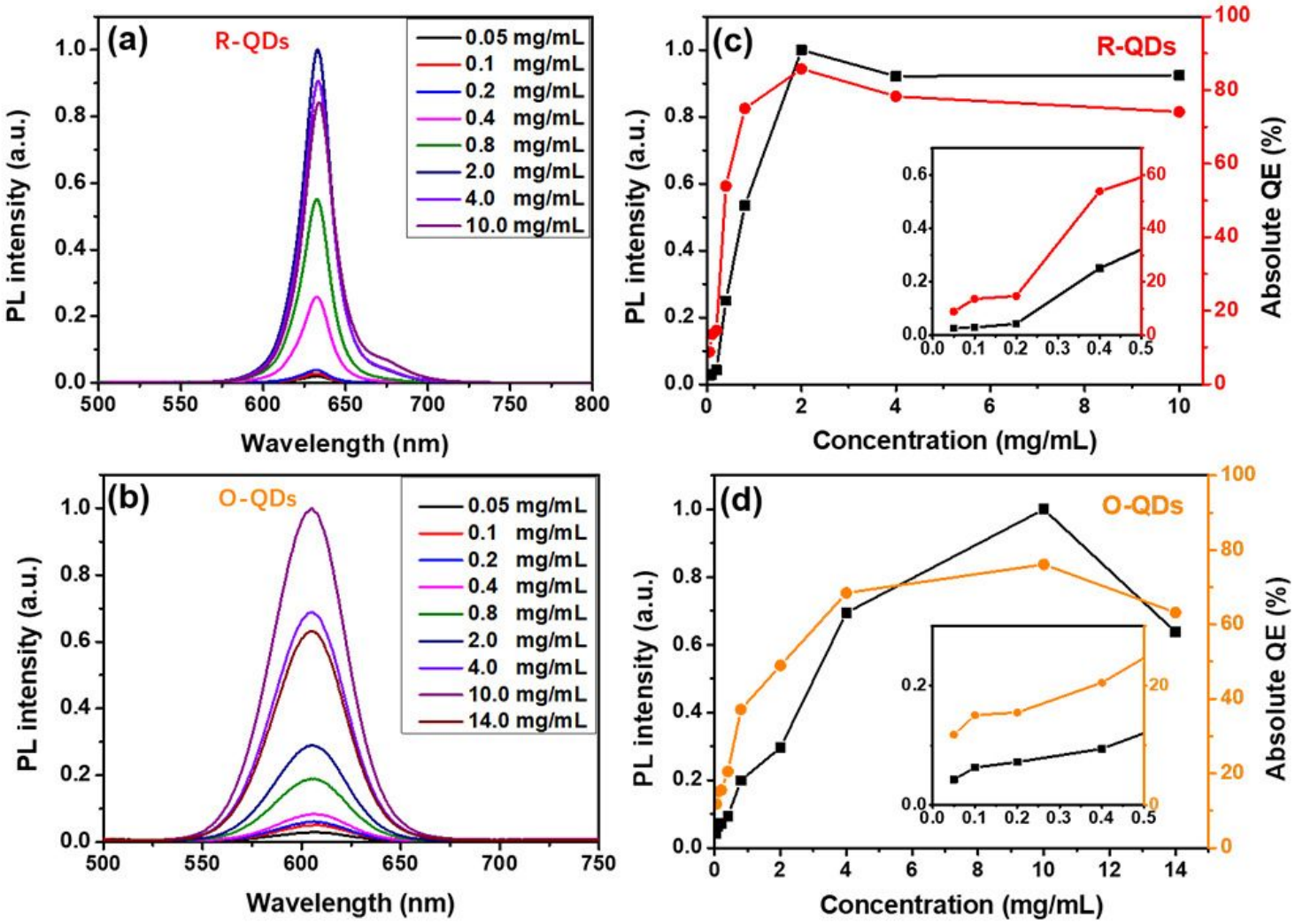

Figure 2

PL spectra of R-QDs (a) and O-QDs (b) based silicone gel thin films. Corresponding PL intensity and QE of R-QDs (c) and O-QDs (d) based silicone gel thin films with different concentrations of QDs.

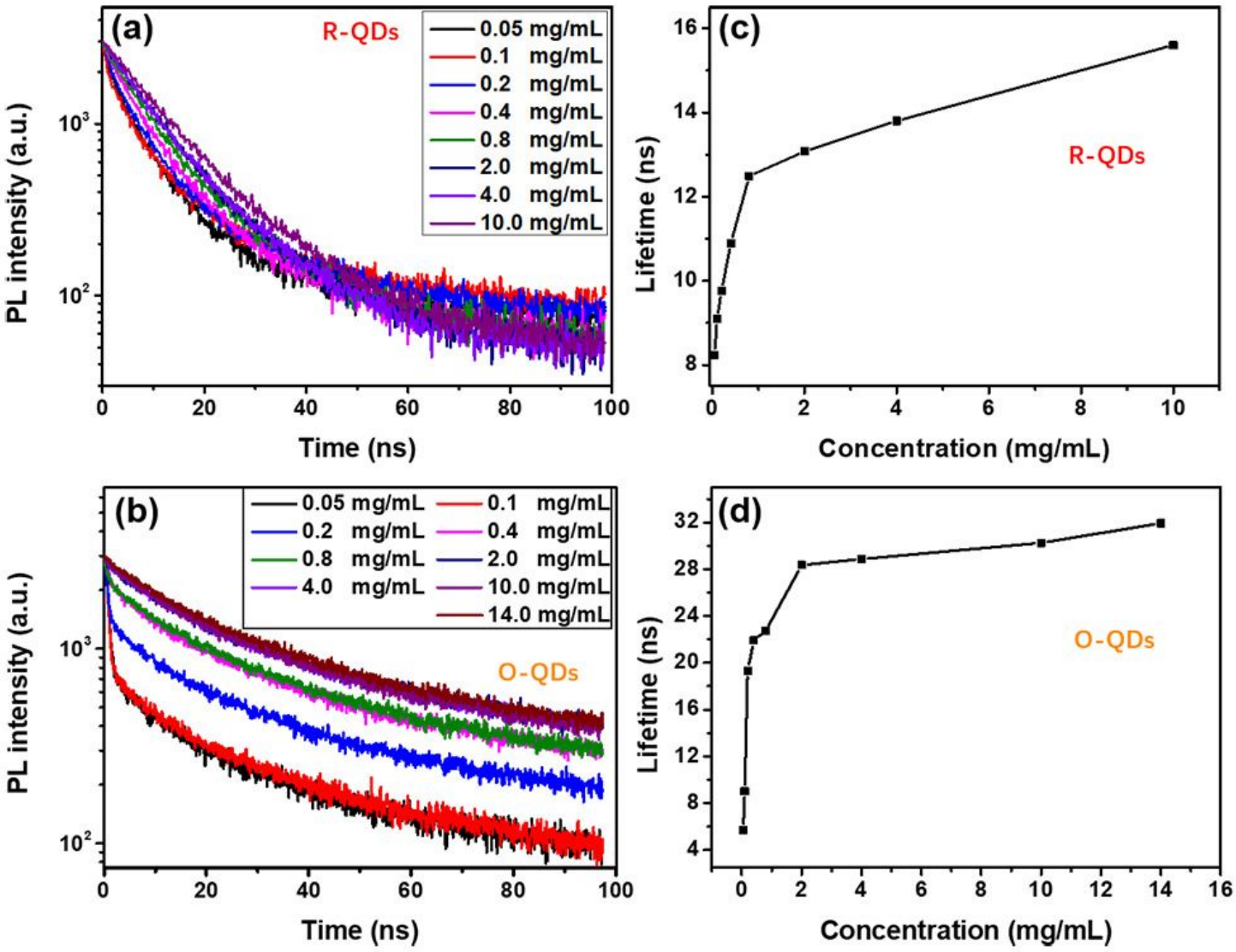

Figure 3

TRPL decay curves of R-QDs (a) and O-QDs (b) based thin films. Lifetimes of R-QDs (c) and O-QDs (d) based silicone gel thin films with different concentrations.

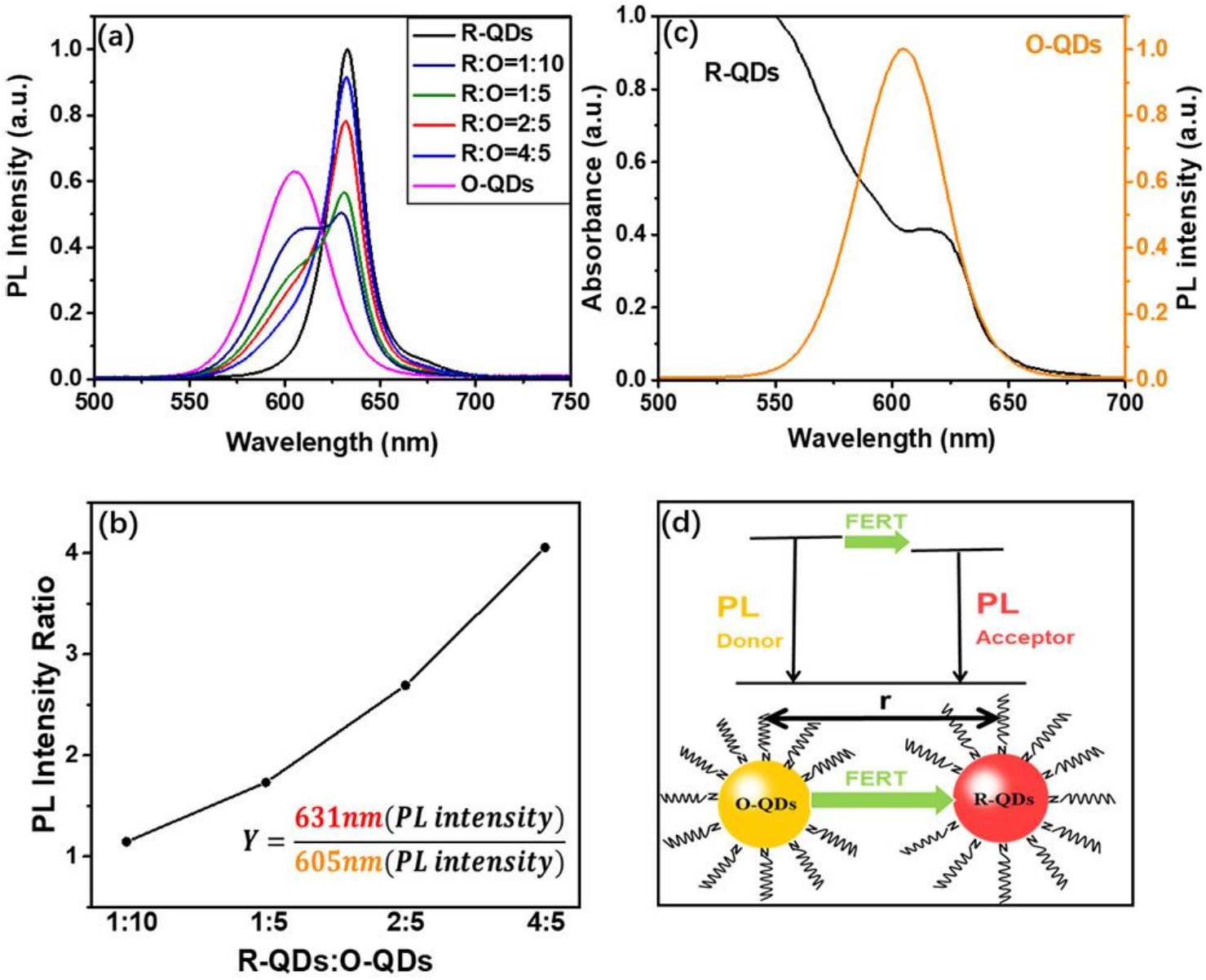

Figure 4

PL spectra of hybrid orange-red QDs silicone thin films with different R-QDs ratio (a) and the hybrid QDs PL peak intensity ratio (b). The overlap of the R-QDs absorption spectrum and O-QDs emission spectrum (c). Schematic diagram of energy transfer in hybrid-QDs (d).

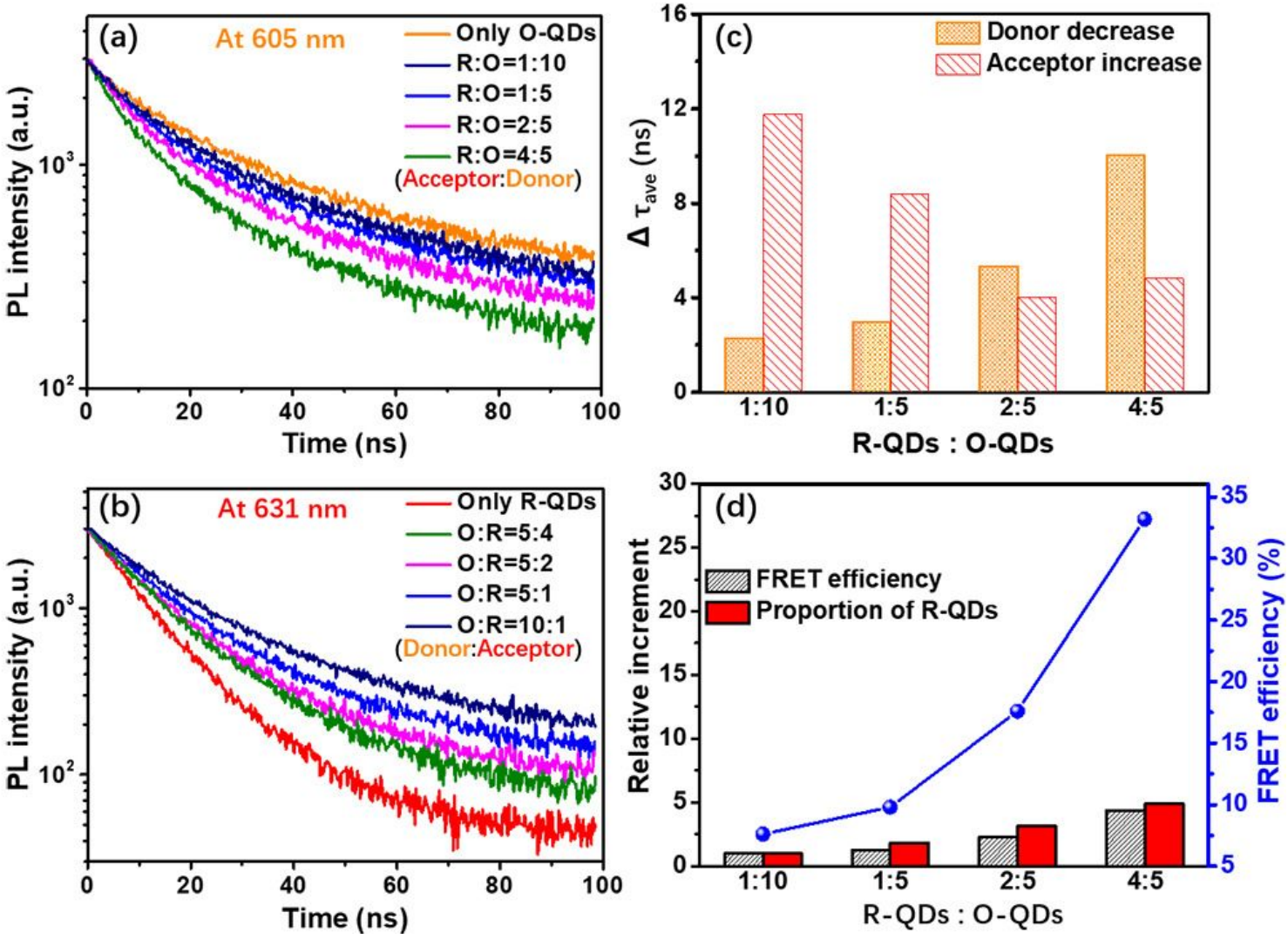

Figure 5

TRPL decay curves of hybrid-QDs thin films with different ratios of R-QDs:O-QDs at donor peak emission wavelength (a) and acceptor peak emission wavelength (b). The variation of donor decrement lifetime and acceptor increment lifetime (c). The comparison of relative increment between in FRET efficiency and R-QDs proportion, and the calculated FRET efficiency under the different ratios of R-QDs:O-QDs (d).

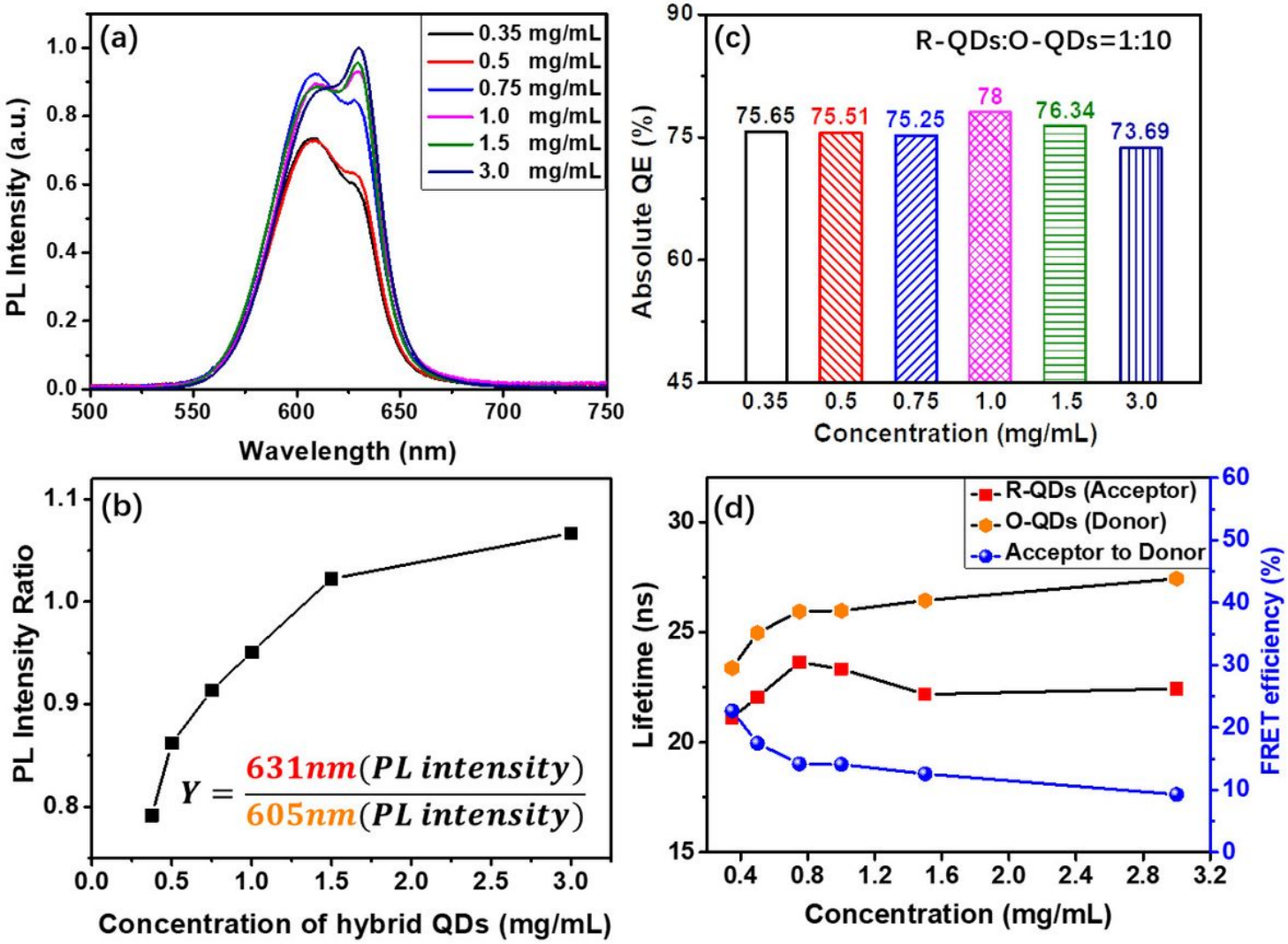

Figure 6

PL spectra of as-prepared hybrid-QDs silicone thin films with different concentrations (a) and their PL peak intensity ratios (b). QE of the as-prepared hybrid-QDs silicone thin films (c). Lifetime of donor (orange dots) or acceptor (red dots), and FRET efficiency (blue dots) under different concentration of hybrid orange-red QDs (d).

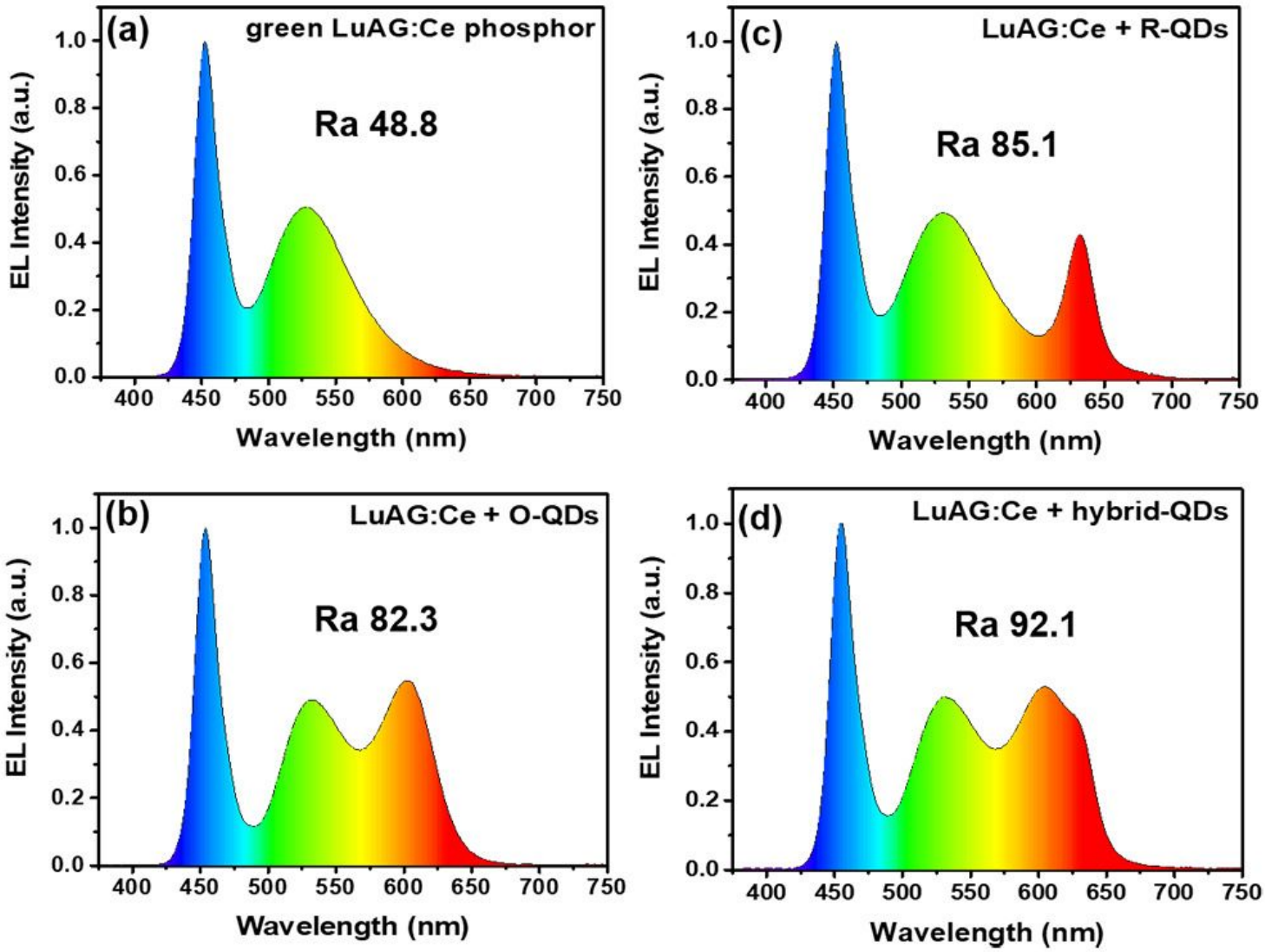

Figure 7

EL spectra of WLEDs packaged with green LuAG:Ce phosphor only (a), LuAG:Ce+R-QDs (b), LuAG:Ce+O-QDs (c), and LuAG:Ce + hybrid-QDs (d).

Supplementary Files

This is a list of supplementary files associated with this preprint. Click to download.

- SupplementaryInformation.doc